

Development of Highly Durable Retinal Prosthesis Using Photoelectric Dyes Coupled to Polyethylene Film and Quantitative In Vitro Evaluation of its Durability

Koichiro Yamashita¹, Tenu Tanaka¹, Toshihiko Matsuo² and Tetsuya Uchida^{*1}

¹ Graduate School of Natural Science and Technology, Okayama University, 3-1-1 Tsushima-naka, Kita-ku, Okayama 700-8530, Japan.

² Graduate School of Interdisciplinary Science and Engineering in Health Systems, Okayama University, 2-5-1 Shikata-cho, Kita-ku, Okayama 700-8558, Japan.

E-mail: tuchida@cc.okayama-u.ac.jp

Received xxxxxx

Accepted for publication xxxxxx

Published xxxxxx

Abstract

Retinal prostheses have been developed to restore vision in blind patients suffering from such diseases as retinitis pigmentosa. In our previous studies, we developed a retinal prosthesis called dye-coupled film by chemical coupling of photoelectric dyes, which absorb light and then generate electrical potential, with a polyethylene film surface. The dye-coupled film is nontoxic, and we recovered the vision of a monkey with macular degeneration. The amount of dye on the dye-coupled film, however, decreased to one-third after five months in the monkey's eye. The photoelectric dye consists of a cation with photoresponsivity and a bromide ion (Br^-). Therefore, an anion-exchange reaction could be applied to the dye-coupled film to improve its durability. In this study, the anion-exchange reaction was conducted using bis(trifluoromethanesulfonyl)imide ion (TFSI^-), which has lower nucleophilicity than Br^- . First, the long-term durability was examined without using animal subjects and in a short period. Subsequently, an elemental analysis was performed to confirm the exchange between Br^- and TFSI^- , and chemical properties, such as photoresponsivity and durability, before and after the anion exchange, were evaluated. It was quantitatively confirmed that the long-term durability of dye-coupled films can be evaluated in an in vitro environment and in a short period of one-thirtieth by utilizing a saline solution at 60°C , compared with an in vivo environment. In addition, the durability of the dye-coupled film with TFSI^- was improved to 270%–320% compared with that of the dye-coupled film with Br^- .

Keywords: retinal prosthesis, photoelectric dye, polyethylene film, retinitis pigmentosa, durability

1. Introduction

The retina consists of a photoreceptor cell layer, a bipolar cell layer, and a ganglion cell layer. The horizontal and amacrine

cells are arranged in the direction perpendicular to the bipolar cells within the bipolar-cell layer. The photoreceptor cell layer is the starting point of vision because it receives the light entering the eye and then generates an electrical signal, that is,

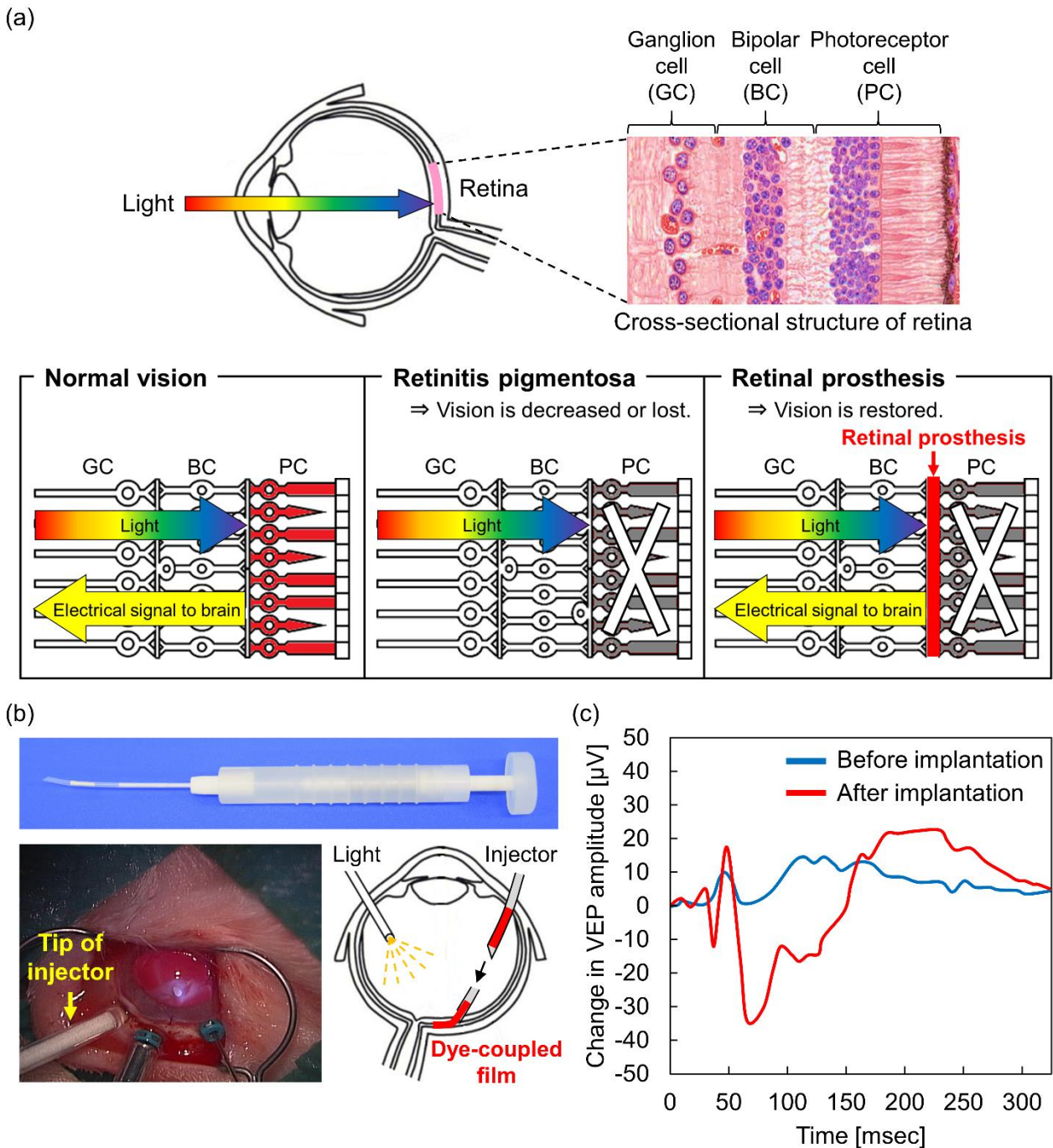


Figure 1. (a) Structure of retinal tissues and visual information processing. Retina consists of a ganglion cell (GC) layer, a bipolar cell (BC) layer, and a photoreceptor cell (PC) layer. In normal vision, the photoreceptor cells convert light to electrical signal, which is then transferred to the brain as visual information. Retinitis pigmentosa is a disease in which the photoreceptor cells are gradually degenerated. Therefore, the visual information does not reach the brain, which ultimately leads to blindness. Retinal prostheses, which can stimulate living retinal tissues in substitution for the photoreceptor cells, have been developed to restore vision. (b) The minimally invasive injector developed for the dye-coupled film. The operability had been confirmed using rabbit eyes. The dye-coupled film is loaded in the tip of the injector, and then it is directly implanted into the subretinal space. (c) Visual evoked potential (VEP) measured in the implantation test into monkey eye. The blue line and the red line represent the VEP before and after the dye-coupled film was implanted, respectively.

depolarization due to the decrease in the release of glutamate, thereby leading to the activation of the bipolar cell. The loss of the photoreceptor cell layer causes retinitis pigmentosa, a

disease that causes blindness [1, 2]. Retinal prostheses, which can provide electrical stimulation to living retinal tissues in

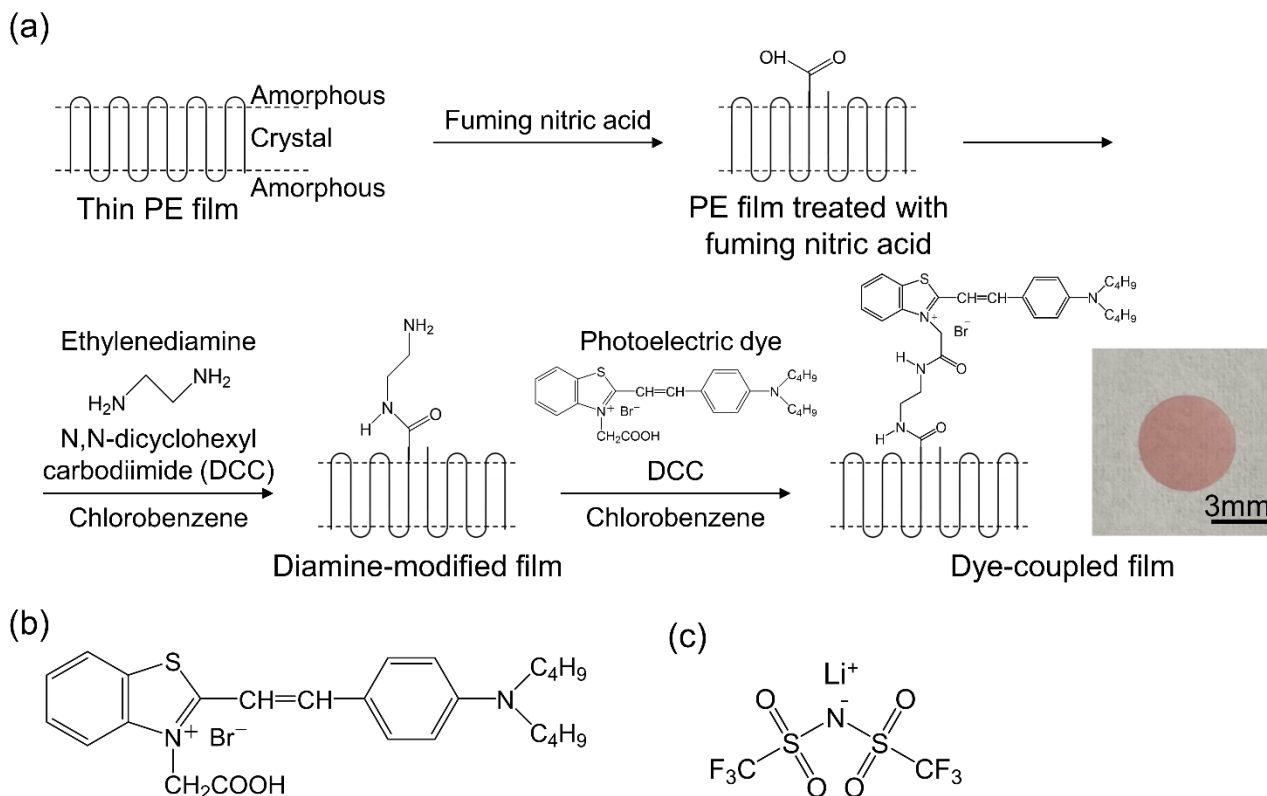


Figure 2. (a) The synthesis process and the image of the dye-coupled film. Chemical structures of (b) the photoelectric dye and (c) a lithium bis(trifluoromethanesulfonyl)imide (LiTFSI).

substitution for the photoreceptor cell layer, have been developed to treat retinitis pigmentosa (Figure 1(a)).

In the USA, the Argus II retinal prosthesis system (Second Sight Medical Products, Sylmar, CA, USA) has been approved by the U.S. Food and Drug Administration (FDA) [3-5]. In addition, the Retina Implant Alpha AMS (preceding Alpha IMS, Retina Implant AG, Aachen, Germany) has obtained the CE mark in the European market [6-8]. These artificial devices utilize a multielectrode array system. The Argus II retinal prosthesis system divides a camera-captured image into 60 pixels, and then, stimulates the living retinal tissues by outputting an electrical current, corresponding to a grayscale tone in each pixel, from 60 electrodes implanted in the epiretinal space. The Retina Implant Alpha AMS has a multielectrode array of 1500 units, and each unit consists of a light-sensitive micro photodiode, an amplifier, and an electrode. In each unit, light sensed by the photodiode is amplified, and then, electrical current is output from the electrode to stimulate the retinal cells. The electrode array system, however, has some disadvantages, including its high price and the need for an external electromotive force from a power control unit to output voltage pulses at the electrodes. In addition, the surgical implantation of these devices requires sophisticated techniques. Therefore, there is a need to develop a retinal prosthesis that can overcome these problems.

Since a photoelectric dye [9, 10], which absorbs light and then converts photon energy to electric potential, has been previously shown to stimulate retinal neurons [11], we were interested in developing a retinal prosthesis using photoelectric dyes. Photoelectric dyes cannot be implanted in the retina because of their powdery nature. Therefore, we selected a thin polyethylene (PE) film as the substrate. It was, however, difficult to chemically modify the PE film surface because of the high stability of PE. We had previously developed a new method to selectively introduce carboxyl moieties to folding portions of PE molecular chains that exist on the PE film surface [12, 13]. Subsequently, a synthesis process for coupling the photoelectric dyes to carboxyl moieties was optimized, which led to the development of the Okayama University-type retinal prosthesis (OUReP), i.e., the dye-coupled film (Figure 2(a)) [14-17]. All biological safety tests for medical devices have been completed, and it was proved that the dye-coupled film has no toxicity. It was also shown that vision of retinal dystrophic rats (RCS rats) was recovered by implanting the dye-coupled film into the eyes [18-21]. In addition, the minimally invasive injector had been developed to safely and easily implant the dye-coupled film into subretinal space by vitreous surgery, and then the operability had been ensured by using rabbit eyes as shown in Figure 1(b) [22]. As the final stage toward human clinical trials, the dye-coupled film was implanted into monkey eye

with macular degeneration to clarify its effectiveness. Visual evoked potential (VEP), which is the electrical signal recorded at the scalp over the occipital cortex in response to light stimulus, was measured to investigate whether the dye-coupled film works properly as an artificial retina (Figure 1(c)). The amplitude of VEP, which had been reduced due to macular degeneration, recovered one month after the implantation, and then maintained its level over five months, which demonstrates the effectiveness of the dye-coupled film [23, 24]. It was also found that the dye amount existing on the film surface was gradually decreased during five months of the implantation. Consequently, a current problem of the dye-coupled film toward industrialization is its long-term durability.

The photoelectric dye consists of a cation with photoresponsivity and a bromide ion (Br^-) (Figure 2(b)). We focused on anion-exchange reactions that can improve such chemical properties as thermal stability, hydrophilicity, and ionic conductivity [25, 26]. It has been reported that, in thermal gravimetric analysis, the temperature at which a sample starts to experience weight loss increases as the nucleophilicity of anions decreases [27]. In other words, the exchange to anions with lower nucleophilicity is expected to stabilize the chemical structure of the dye-coupled film. In this study, lithium bis(trifluoromethanesulfonyl)imide (LiTFSI, Figure 2(c)) was selected for the anion exchange to develop a next-generation retinal prosthesis with TFSI^- instead of Br^- , which is expected to exhibit long-term durability. Since it is difficult to conduct implantation tests in monkeys' eyes over five months to evaluate the long-term durability, the amount of dye on the dye-coupled film before and after the implantation test was quantitatively evaluated. Subsequently, an accelerated aging (AA) durability test in phosphate-buffered saline at high temperatures was conducted to evaluate the long-term durability of the dye-coupled film in an *in vitro* environment and in a short period [28-30]. Then, the AA durability was quantitatively compared with the change in the amount of dye during the implantation test. Next, elemental analyses were performed on the dye-coupled film before and after the anion-exchange reaction to confirm the occurrence of the reaction. Finally, the photoresponsivity and the durability of the dye-coupled film before and after the anion-exchange reaction were evaluated.

2. Experimental section

2.1. Preparation of normal dye-coupled film

A piece of Teflon film was placed on an aluminum plate, and high-density polyethylene (HDPE) powder (30 mg, $M_w = 1.5 \times 10^5$) was placed on the center of the plate. The HDPE powder was then sandwiched with another Teflon film and aluminum plate. Vacuum pressing was implemented at 160°C using a vacuum heating press (IMC-11FD, Imoto machinery

Co.). After pressing, the sample was rapidly cooled in ice water to prepare a thin crystallized PE film (thickness: $30 \pm 5 \mu\text{m}$), which was added along with fuming nitric acid (100 mL) into a four-neck flask equipped with a Dimroth condenser. The flask was placed in an oil bath at 80°C for 14 min. The film treated with fuming nitric acid was washed with ultrapure water (Direct-Q 3 UV, Merck Millipore) until the pH of the water reached neutral, and was then dried for 24 h. The film was immersed in a stoppered flask containing chlorobenzene (75 mL), ethylenediamine (2.6 μL , 4.0×10^{-5} mol), and N,N'-dicyclohexylcarbodiimide (DCC, 8.25 mg, 4.0×10^{-5} mol). The contents were stirred at 50 rpm using a shaking water bath (NTS-4000AM, EYELA) and reacted at 35°C for 48 h. After the reaction, the film was washed with chlorobenzene. The photoelectric dye (20 mg, 4.0×10^{-5} mol), chlorobenzene (75 mL), and DCC (8.25 mg, 4.0×10^{-5} mol) were added in a stoppered flask. The photoelectric dyes were dispersed by ultrasonic irradiation for 30 min using an ultrasonic bath (2510J-MT, BRANSON). The diamine-modified film was then immersed in the flask. The contents were stirred at 50 rpm and reacted at 35°C for 48 h using the shaking water bath. After the reaction, the film was washed with chlorobenzene and ultrapure water, and was then dried.

2.2. Preparation of anion-exchanged dye-coupled film

Lithium bis(trifluoromethanesulfonyl)imide (LiTFSI, 1.0 M) was added in acetonitrile. The normal dye-coupled film was immersed in the solution and reacted in a water bath at 50°C in a dark environment for 3 d. After the reaction, the film was washed with methanol, and was then dried. The dye-coupled film before and after the anion-exchange reaction are named normal dye-coupled film and anion-exchanged (AE) dye-coupled film, respectively.

2.3. Chemical properties

The absorbance spectra of the dye-coupled films were obtained using an UV-vis spectrophotometer with an integrating sphere unit (V-750 and PIV-756, JASCO Corporation, Tokyo, Japan), and the baseline absorbance was obtained using a plain PE film. The absorbance was measured in a wavelength range of 300 to 800 nm. The maximum absorbance between 400 and 600 nm was used to quantitatively compare the amounts of dye on the film. The absorbance spectra of the dye-coupled films before and after the implantation test in the monkey's eye for five months and used for the durability tests (see next section) were measured under the above conditions. The number (N) of dye-coupled films examined after the implantation test is one ($N = 1$). The residual rates of the amount of dye after the implantation test and during the durability tests were calculated using Equation (1) and (2), respectively, as follows:

$$\text{Residual rate of dye amount [\%]} = \frac{\text{Absorbance value after the implantation test [-]}}{\text{Absorbance value before the implantation test [-]}} \times 100 \quad (1)$$

$$\text{Residual rate of dye amount [\%]} = \frac{\text{Absorbance value after standing in saline solution [-]}}{\text{Absorbance value at 0th month [-]}} \times 100 \quad (2)$$

The elemental analyses of the dye-coupled films were evaluated using a scanning electron microscope (SEM; JEOL JSM-IT100) equipped with an energy-dispersive x-ray spectroscopy (EDX) apparatus. The acceleration voltage was 15 keV. The anion-exchange rate was calculated by ZAF correction method.

The light-induced electrical potential on the dye-coupled films was measured with a scanning Kelvin probe (SKP) system (SKP5050, KP Technology, Ltd., Highlands and Islands, UK) [31-33]. The entire measuring system was placed in a humidity-controlled box. The light intensity was controlled by a surface photovoltage spectroscopy (SPS) module (SPS040, KP Technology). Incident light was irradiated while gradually increasing the light intensity, and the change in surface electrical potential was measured. The electrical potential value at a light intensity of 2500 arbitrary unit (A.U.), which is nearly equal to 300 lux, was used for comparison.

2.4. Durability tests

Nine normal dye-coupled films having different absorbance were used for the durability test using phosphate-buffered saline (PBS, pH 7.2, containing 0.90 w/v% sodium chloride, 0.0726 w/v% di-sodium hydrogenphosphate heptahydrate, and 0.021 w/v% potassium dihydrogenphosphate) at 35°C in real-time (RT). The normal dye-coupled film and PBS were put in a sample tube and allowed to stand in a water bath at 35°C in a dark environment for seven months. The absorbance spectra were measured in months 0, 1, 3, 5, and 7. Five normal dye-coupled films and five AE dye-coupled films were employed for the AA durability test using PBS at 60°C. The normal or the AE dye-coupled film and PBS were put in a sample tube, which was then placed in a water bath at 60°C and allowed to stand in a dark environment for 7 or 21 days. The absorbance spectra were measured every day.

An accelerated aging factor (AAF) between the RT and the AA durability tests can be approximated by the 10-degree rule (Equation (3)), developed around the collision theory-based Arrhenius model [28-30].

$$AAF = Q_{10}^{(T_{RT}-T_{AA})/10} \quad (3)$$

where T_{RT} and T_{AA} are the temperatures in the RT and AA durability tests, respectively. In addition, Q_{10} of 2 was adopted as the coefficient of the reaction rate, which is appropriate for a wide range of medical polymers [29].

For the normal dye-coupled film, the correlation between the experimental results and the prediction obtained using

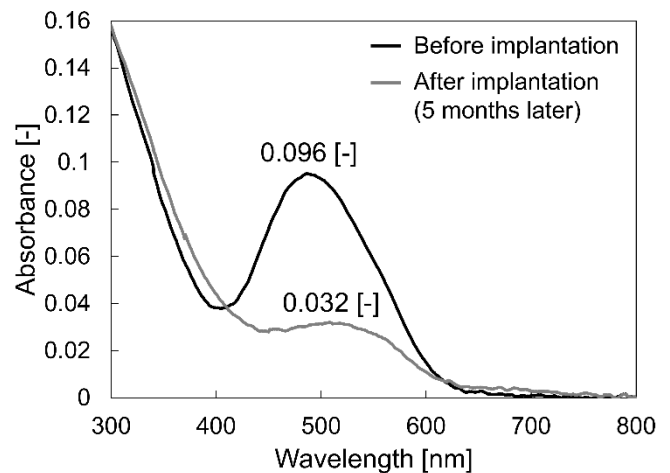


Figure 3. Absorbance spectra of the dye-coupled film before (black line) and after (gray line) five months of implantation test in the monkey's eye. One dye-coupled film was quantitatively evaluated after the implantation test.

AAF was quantitatively evaluated. Next, the temporal changes in the residual rate of the amount of dye on the implantation in the monkey's eye (normal dye-coupled film), the RT durability test in PBS at 35°C (normal dye-coupled film), and the AA durability test in PBS at 60°C (normal and AE dye-coupled films) were compared.

3. Results and discussion

3.1. Dye amount on the dye-coupled film implanted in monkey's eye

The dye amount on the dye-coupled film was quantitatively evaluated using the UV-vis spectroscopy. The absorbance spectra of the dye-coupled film before and after the implantation test in the monkey's eye are shown in Figure 3. Since the color of the dye-coupled film is red, it absorbs in the green wavelength range (495–570 nm), which is the complementary color. The maximum absorbance value between 400 and 600 nm was used to compare the dye amount on the film. The maximum values of the dye-coupled film before and after the implantation test were 0.096 [-] and 0.032 [-], respectively. The residual rate of the dye amount after the implantation test calculated using Equation (1) was 33.5%.

3.2. Durability tests conducted in an in vitro environment and in a short period

3.2.1. Durability test in real-time using PBS at 35°C

Durability tests were conducted in PBS at 35°C, which is a condition similar to that of an in vivo environment, to clarify, without using animal subjects, how the amount of dye on the film changes overtime during the implantation in the monkey's eye. In addition, nine dye-coupled films having different absorbance were selected to investigate the effect of

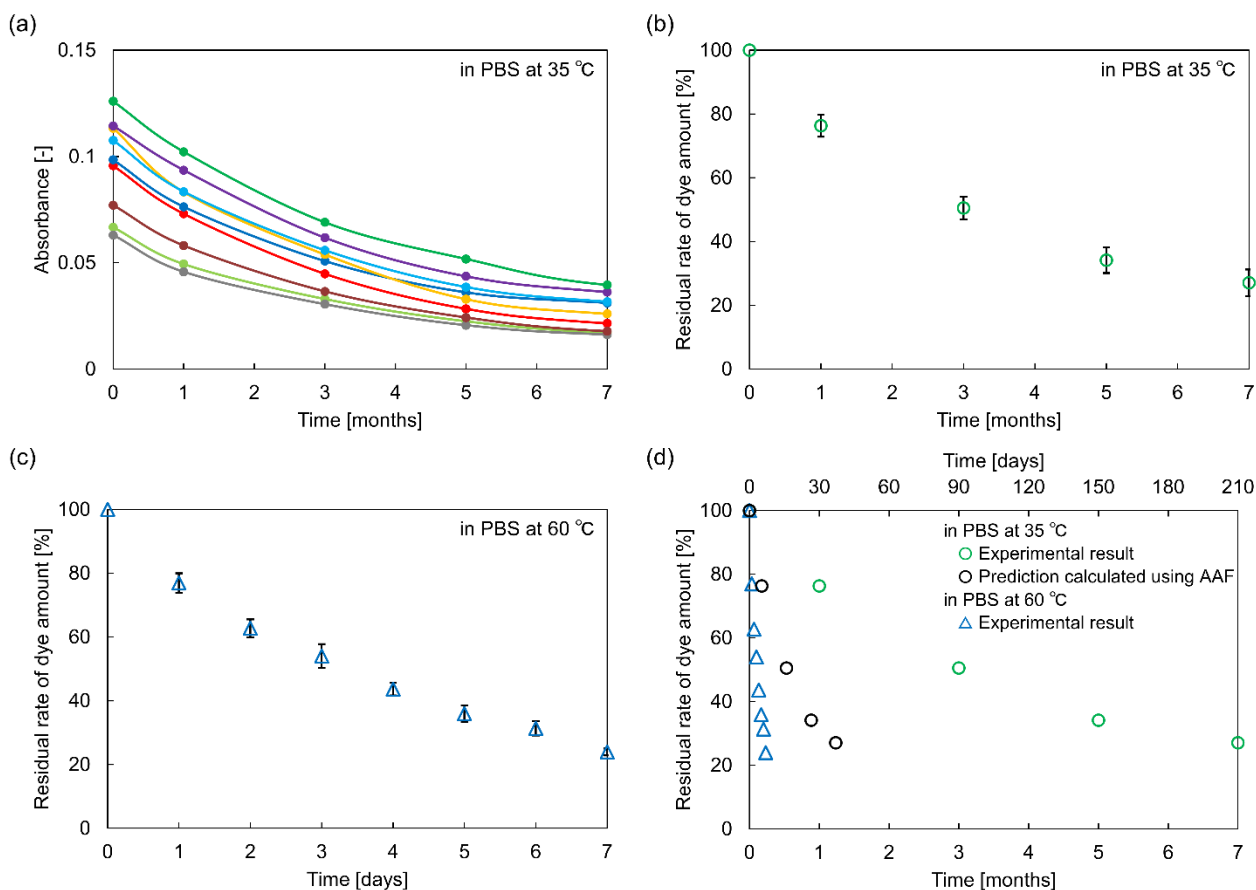


Figure 4. (a) Comparison of the durability tests on nine dye-coupled films with different amounts of dyes in PBS at 35°C for seven months. Each plot represents the maximum absorbance extracted from the respective absorbance spectra. (b) Average residual rates of dye amount and their standard deviations calculated from Figure 4(a). (c) Average residual rates of amounts of dye and their standard deviations for durability tests on five dye-coupled films in PBS at 60°C for seven days. (d) Comparison between durability tests in PBS at 35°C (green circles) and 60°C (blue triangles). The black circles represent the predictions obtained by dividing the experimental result in PBS at 35°C (green circles) by 5.66 (AAF). The time scales of the horizontal axes are the same. The residual rates were calculated using Equation (2).

the initial amount of dye on its change with time. The maximum absorbance of the nine dye-coupled films after standing in PBS for 0, 1, 3, 5, and 7 months are shown in Figure 4(a). The absorbance of each of the nine dye-coupled films gradually decreased while approaching a steady state. The samples with higher initial absorbance exhibited higher absorbance on the seventh month, and those with lower initial absorbance showed lower absorbance on the seventh month. Subsequently, to elucidate the correlation in the temporal changes in the amount of dye among the nine dye-coupled films, all the absorbance were converted to residual rates of the amount of dye using Equation (2). The average values of the residual rates and their standard deviations are shown in Figure 4(b). The changes recorded with time in the nine dye-coupled films were similar because the standard deviations were small. Therefore, it was ascertained that temporal changes can be compared using the residual rate of the amount of dye, irrespective of the initial absorbance. In addition, the residual rate of the amount of dye after standing in PBS at 35°C for five months was 34.1% and the residual rate after

being implanted in the monkey's eye for five months was 33.5%. Since the in vivo residual rates were the same as that in PBS at 35°C, it can be concluded that the amount of dye decreases at the same rate in both conditions, which demonstrates that the change in the amount of dye overtime in an in vivo environment can be reproduced without using animal subjects.

3.2.2. Accelerated aging durability test using PBS at 60°C

There was a correlation between the temporal changes in residual rate in the monkey's eye and those in the PBS at 35°C. Nevertheless, it is necessary to evaluate the long-term durability in a short period. We, therefore, focused on a method to decompose the dye-coupled film in a short period at a high temperature [28-30]. Figure 4(c) shows the temporal change in the residual rate of the dye-coupled film in PBS at 60°C. It reached 35.9% on the fifth day, which is almost the same value obtained in the monkey's eye and in PBS at 35°C in the fifth month. Hence, it was ascertained that the residual

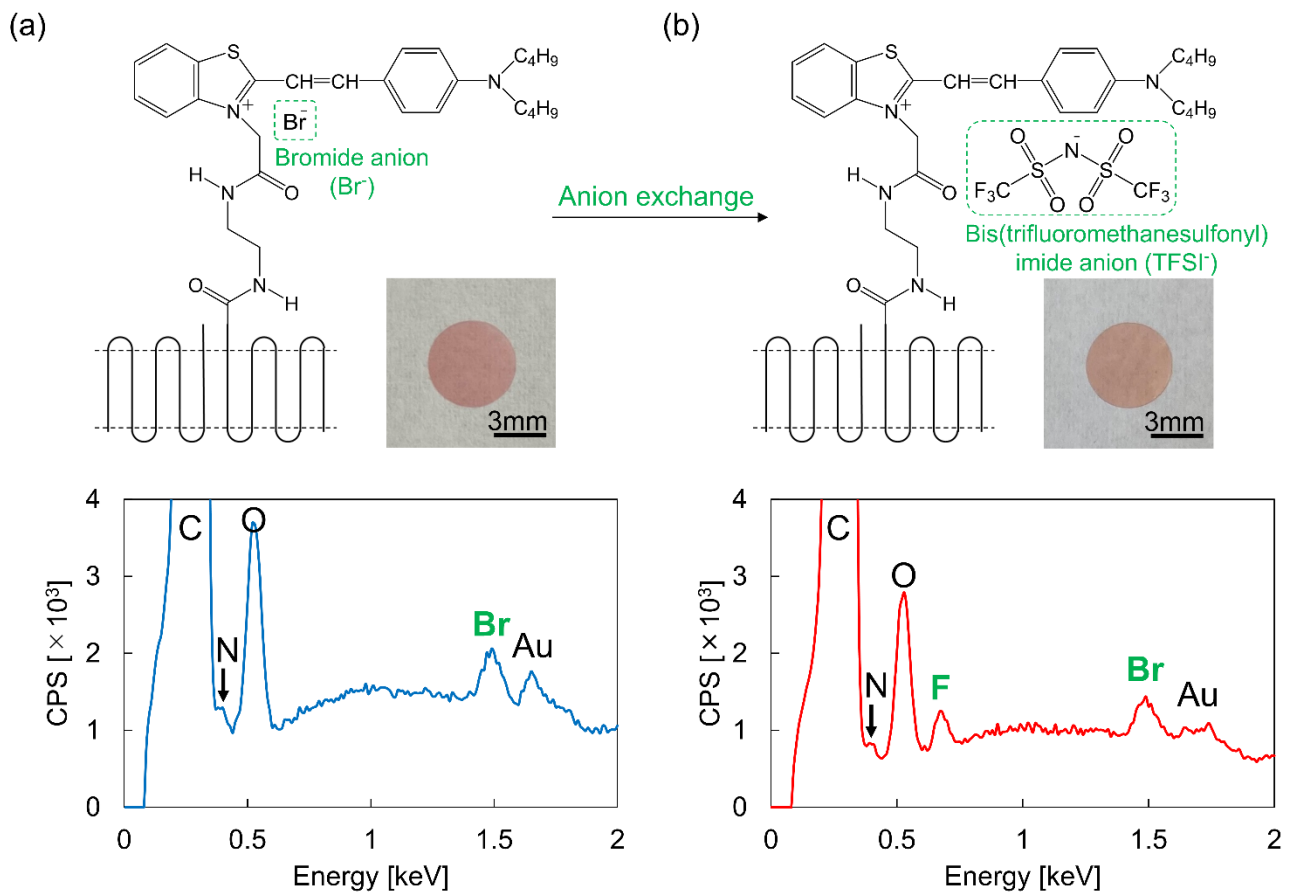


Figure 5. The chemical structures, images, and elemental analyses of (a) the normal dye-coupled film and (b) the anion-exchanged (AE) dye-coupled film.

rates of the amount of dye after standing for one month in the monkey's eye or PBS at 35°C were the same as those in PBS at 60°C after standing for one day. The AAF between the experimental results was assumed to be ~30 because one day at 60°C corresponds to 30 days at 35°C.

The AAF between the RT durability test at $T_{RT} = 35^\circ\text{C}$ and the AA durability test at $T_{AA} = 60^\circ\text{C}$ was calculated for the prediction as follows:

$$AAF = Q_{10}^{(T_{RT}-T_{AA})/10} = 2^{\Delta T/10} = 5.66 \quad (4)$$

AAF = 5.66 implies that one day at 60°C (T_{AA}) is equivalent to 5.66 days at 35°C (T_{RT}). The acceleration factor (~30) between the experimental results in PBS at 35°C and 60°C was much larger than that (5.66) predicted based on the 10-degree rule. As shown in Figure 4(d), the residual rate of the amount of dye in the experiment using PBS at 60°C (blue triangles) rapidly decreased, compared with the prediction (black circles) obtained by dividing the experimental result of the PBS at 35°C (green circles) by 5.66 (AAF). The difference is attributed to the low thermal stability of photoelectric dyes, hydrolysis of amide bonds, and diffusion in PBS. It was reported that the activation energy in the Arrhenius equation becomes large at higher temperatures [34]. In other words, the

thermal degradation of a material accelerates nonlinearly as temperature increases. Herein, the photoelectric dye began to decompose in the air at ~125°C, as shown in Figure S1 of Supporting Information. In addition, the photoelectric dyes were selectively coupled to the film surface. Therefore, diffusion at the solid-liquid interface between the dyes coupled to the film surface and PBS increased as T_{AA} increased, which accelerates the degradation of such chemical bonds as the amide bonds and the dye molecules. Therefore, the reaction rate coefficient Q_{10} for the dyes coupled to the film surface is assumed to be greater than 2 because the dyes are likely to be thermally unstable and are affected by the diffusion in PBS at 60°C compared with ordinal medical polymers, which obey the 10-degree rule with $Q_{10} = 2$. The larger Q_{10} resulted in a higher AAF. It was experimentally confirmed that the durability of the dye-coupled film for one day in PBS at 60°C corresponds to that for one month in PBS at 35°C, and its AAF is ~30. It also demonstrates that the long-term durability of the dye-coupled film can be evaluated in an in vitro environment and in a short period of one-thirtieth by utilizing PBS at 60°C.

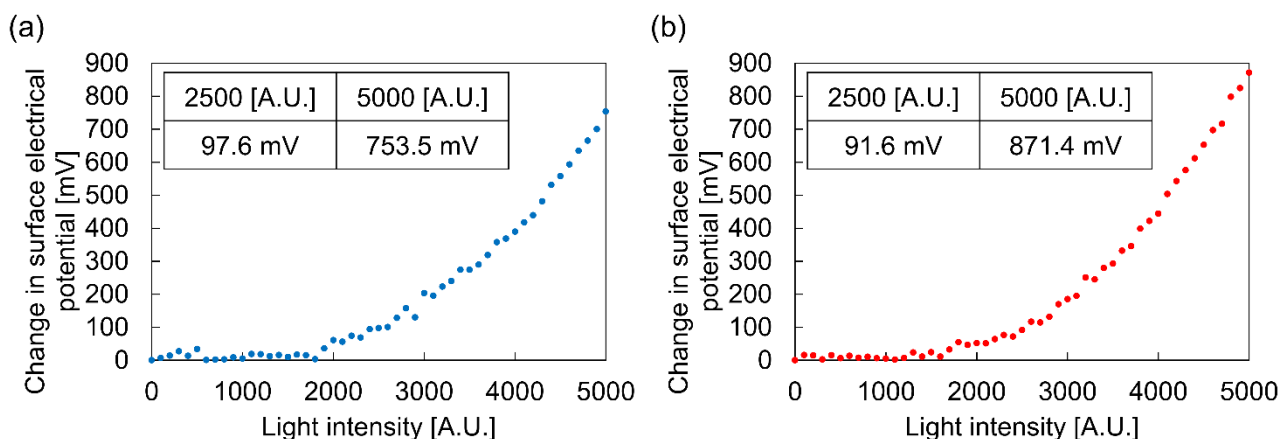


Figure 6. Light intensity dependence of light-induced surface electrical potential on (a) the normal dye-coupled film and (b) the anion-exchanged (AE) dye-coupled film.

3.3. Chemical properties of the dye-coupled film before and after anion-exchange reaction

3.3.1. Elemental analysis

The chemical structures, images, and elemental analyses of the normal dye-coupled film and the AE dye-coupled film are shown in Figure 5(a) and 5(b), respectively. Bromine (Br) is the characteristic element in the normal dye-coupled film, and fluorine (F), which stems from TFSI, is the characteristic element in the AE dye-coupled film. The $K\alpha$ lines of carbon (C), nitrogen (N), oxygen (O), and fluorine (F) would be expected to appear around 0.277, 0.392, 0.525, and 0.677 keV, respectively. In addition, a peak derived from the $L\alpha$ line of the Br element should be obtained around 1.48 keV [35]. In the elemental analysis of the normal dye-coupled film, no peak derived from the $K\alpha$ line of the F element was observed, and the peak derived from the $L\alpha$ line of Br appeared around 1.48 keV. This indicated that the anion-exchange reaction could be applied to the normal dye-coupled film because Br anions were not lost during the preparation process. The peak derived from the $K\alpha$ line of F was obtained around 0.677 keV on the AE dye-coupled film. Therefore, it was confirmed that the anion-exchange reaction occurred. However, since the peak of Br was also present in the elemental analysis of the AE dye-coupled film, Br anions were not completely exchanged. The exchange rate from Br^- to TFSI $^-$ was estimated to be 36.3%, which is most likely because TFSI $^-$ has lower nucleophilicity and larger steric hindrance than Br^- due to its larger molecular size [27].

3.3.2. Light-induced surface electrical potential

In our previous study, photoresponsivity of the dye-coupled film was measured by using the SKP system [31–33]. The light intensity dependence of the light-induced electrical potential on the normal dye-coupled film and the AE dye-coupled film

are shown in Figure 6(a) and 6(b), respectively. Both dye-coupled films before and after the anion exchange showed photoresponsivity. The electrical potential was dependent on the light intensity and became larger as the irradiated light became brighter. In other words, the anion-exchange method allowed changing Br anions to TFSI anions without losing the photoresponsivity of the cation, and the AE dye-coupled film exhibited photoresponsivity even after the anion-exchange reaction. It has been previously shown that retinal photoreceptor cells of a mouse generate electrical potential of several tens of mV in response to external light stimulus [36]. In the present study, the surface electrical potential was around 95 mV at 2500 A.U. (300 lux), which is nearly equal to sunset light. Therefore, it can be assumed that the dye-coupled film can generate sufficient electrical potential to stimulate retinal tissues in substitution of photoreceptor cells.

3.3.3. Accelerated aging durability test using PBS at 60°C

Figure 7 shows the AA durability test in PBS at 60°C for the AE dye-coupled film (red squares). For comparison, the temporal changes in the residual rate of the normal dye-coupled film on the implantation in the monkey's eye (black rhombuses), the RT durability test in PBS at 35°C (green circles), and the AA durability test in PBS at 60°C (blue triangles) are also shown in Figure 7. The residual rates of the normal dye-coupled film reached about 34% on the fifth day or the fifth month under any condition. On the other hand, the residual rate of the AE dye-coupled film reached 33.0% on the sixteenth day by standing in PBS at 60°C. In addition, the half decay periods of the normal and the AE dye-coupled films were three and eight days, respectively. Therefore, the long-term durability of the AE dye-coupled film was improved by 270%–320% relative to that of the normal dye-coupled film. The elemental analysis of the AE dye-coupled film after standing in PBS at 60°C for 21 days is shown in Figure 8. It

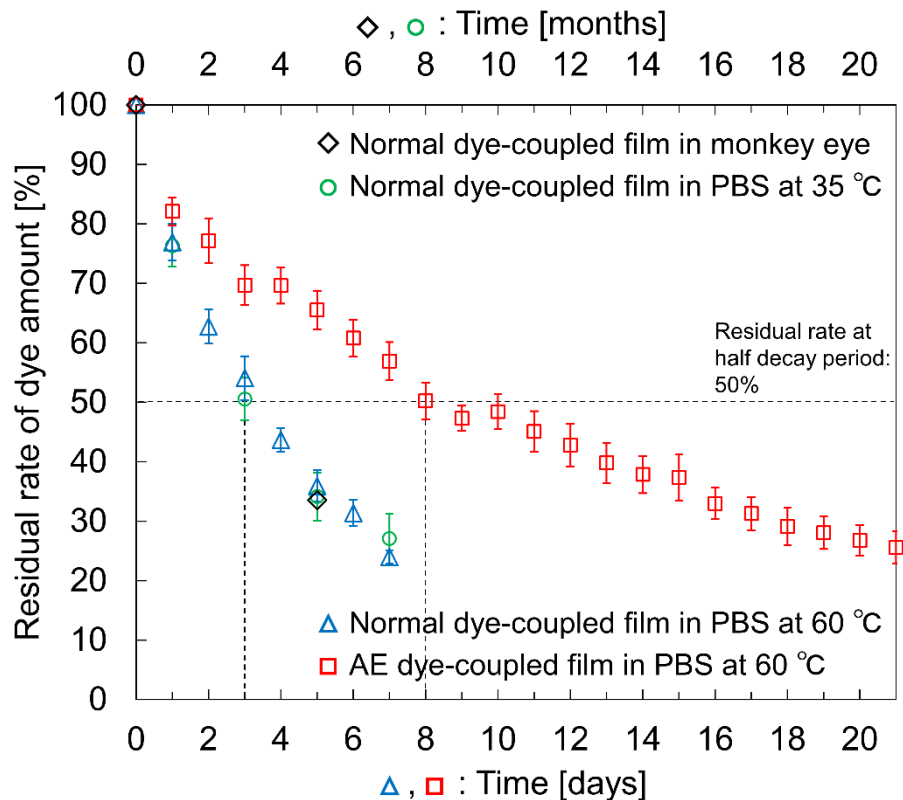


Figure 7. Comparison of durability tests using the normal dye-coupled film and the anion-exchanged (AE) dye-coupled film. The black rhombuses, green circles, and blue triangles represent the temporal changes in the residual rate of the amount of dye in the implantation test in the monkey's eye, the real-time (RT) durability test in PBS at 35°C, and the accelerated aging (AA) durability test in PBS at 60°C using the normal dye-coupled film, respectively. The red squares represent the residual rate of the amount of dye with time on the AA durability test in PBS at 60°C using the AE dye-coupled film. The residual rates were calculated using Equation (2). The time scale of the horizontal axes was set such that one day in the AA durability test corresponds to one month in the RT durability test.

was confirmed that TFSI⁻ was present on the film surface, even after the durability test, because the peak corresponding to the F element was present. In addition, the rate of exchange from Br⁻ to TFSI⁻ was 25.6%. This result indicates that the

effect of TFSI⁻ remained throughout the period of the durability test.

4. Conclusions

Through a five-month implantation test in a monkey's eye, it was obtained that the amount of dye on a normal dye-coupled film gradually decreases. To improve the long-term durability of the normal dye-coupled film, we conducted anion-exchange reactions. Generally, the evaluation of the durability using animal subjects is costly and time-consuming. These problems were overcome in this study; we obtained that the temporal change in the amount of dye in a monkey's eye can be reproduced in an in vitro environment and in a short period of one-thirtieth by standing in PBS at 60°C. In addition, the condition to exchange Br⁻, the anions of the normal dye-coupled film, to TFSI⁻ was established, and an AE dye-coupled film was developed. The long-term durability of the AE dye-coupled film was improved by 270%–320% relative to that of the normal dye-coupled film. The anion-exchange reaction effectively improved the long-term durability of the dye-coupled film, which resulted in the development of a next-generation retinal prosthesis.

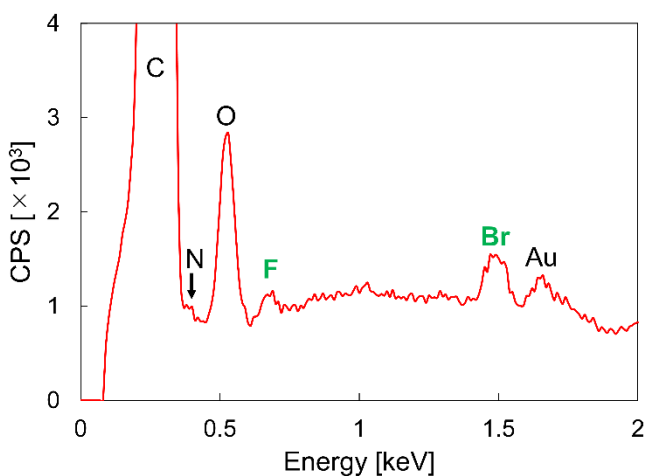


Figure 8. Elemental analysis of the anion-exchanged (AE) dye-coupled film after the accelerated aging durability test in PBS at 60°C for 21 days.

Acknowledgements

This work was supported by JSPS KAKENHI Grant Number JP19J13826.

References

- [1] Matsuo T and Morimoto N 2007 *Br. J. Ophthalmol.* **91** 888
- [2] Tamaki M and Matsuo T 2011 *J. Artif. Organs* **14** 140
- [3] Humayun M S, de Juan E, Jr. and Dagnelie G 2016 *Ophthalmology* **123** S89
- [4] Humayun M S, Dorn J D, da Cruz L, Dagnelie G, Sahel J A, Stanga P E, Cideciyan A V, Duncan J L, Elliott D, Filley E, Ho A C, Santos A, Safran A B, Arditi A, Del Priore L V and Greenberg R J 2012 *Ophthalmology* **119** 779
- [5] da Cruz L, Dorn J D, Humayun M S, Dagnelie G, Handa J, Barale P O, Sahel J A, Stanga P E, Hafezi F, Safran A B, Salzmann J, Santos A, Birch D, Spencer R, Cideciyan A V, de Juan E, Duncan J L, Elliott D, Fawzi A, Olmos de Koo L C, Ho A C, Brown G, Haller J, Regillo C, Del Priore L V, Arditi A and Greenberg R J 2016 *Ophthalmology* **123** 2248
- [6] Stingl K, Bartz-Schmidt K U, Besch D, Braun A, Bruckmann A, Gekeler F, Greppmaier U, Hipp S, Hortdorfer G, Kernstock C, Koitschev A, Kusnyerik A, Sachs H, Schatz A, Stingl K T, Peters T, Wilhelm B and Zrenner E, 2013 *Proc. R. Soc. B* 280
- [7] Stingl K, Bartz-Schmidt K U, Besch D, Chee C K, Cottrill C L, Gekeler F, Groppe M, Jackson T L, MacLaren R E, Koitschev A, Kusnyerik A, Neffendorf J, Nemeth J, Naem M A N, Peters T, Ramsden J D, Sachs H, Simpson A, Singh M S, Wilhelm B, Wong D and Zrenner E 2015 *Vision Research* **111** 149
- [8] Stingl K, Schippert R, Bartz-Schmidt K U, Besch D, Cottrill C L, Edwards T L, Gekeler F, Greppmaier U, Kiel K, Koitschev A, Kühlewein L, MacLaren R E, Ramsden J D, Roeder J, Rothermel A, Sachs H, Schröder G S, Tode J, Troelenberg N and Zrenner E 2017 *Front. Neurosci.* **11** 445
- [9] Okamoto K, Matsuo T, Tamaki T, Uji A and Ohtsuki H 2008 *J. Artif. Organs* **11** 45
- [10] Liu S, Matsuo T, Hosoya O and Uchida T 2017 *J. Ocul. Pharmacol. Ther.* **33** 149
- [11] Matsuo T 2003 *Acta Med. Okayama* **57** 257
- [12] Tagawa T and Shimamura K 1980 *J. Electron Microsc.* **28** 314
- [13] Uchida T, Ishimaru S, Shimamura K, Uji A, Matsuo T and Ohtsuki H 2005 *Mem. Fac. Eng. Okayama Univ.* **39** 16
- [14] Uji A, Matsuo T, Ishimaru S, Kajiura A, Shimamura K, Ohtsuki H, Dan-oh Y and Suga S 2005 *Artif. Organs* **29** 53
- [15] Uji A, Matsuo T, Uchida T, Shimamura K and Ohtsuki H, 2006 *Artif. Organs* **30** 695
- [16] Tamaki T, Matsuo T, Hosoya O, Tsutsui K M, Uchida T, Okamoto K, Uji A and Ohtsuki H 2008 *J. Artif. Organs* **11** 38
- [17] Matsuo T, Uchida T and Takarabe K 2009 *J. Artif. Organs* **12** 213
- [18] Alamusi, Matsuo T, Hosoya O, Tsutsui K M and Uchida T 2013 *J. Artif. Organs* **16** 343
- [19] Alamusi, Matsuo T, Hosoya O, Tsutsui K M and Uchida T 2015 *J. Artif. Organs* **18** 264
- [20] Alamusi, Matsuo T, Hosoya O and Uchida T 2017 *J. Artif. Organs* **20** 158
- [21] Matsuo T, Uchida T, Yamashita K, Takei S, Ido D, Fujiwara A, Iino M and Oguchi M 2019 *Heliyon* **5** e01936
- [22] Matsuo T, Uchida T, Yamashita K, Matsuo C, Kawakami Y, Hitomi T, Taga K, Sanada T, Yamashita Y and Kuramoto K, 2018 *Anim. Eye Res.* **37** 3
- [23] Shirai H, Mandai M, Matsushita K, Kuwahara A, Yonemura S, Nakano T, Assawachananont J, Kimura T, Saito K, Terasaki H, Eiraku M, Sasai Y and Takahashi M 2015 *PNAS* E81
- [24] Matsuo T, Uchida T, Sakurai J, Yamashita K, Matsuo C, Araki T, Yamashita Y and Kamikawa K 2018 *Artif. Organs* **42** E186
- [25] Hong S H, Tung T T, Trang L K H, Kim T Y and Suh K S 2010 *Colloid Polym. Sci.* **288** 1013
- [26] Chen M, Dugger J W, Li X, Wang Y, Kumar R, Meek K M, Uhrig D W, Browning J F, Madsen L A, Long T E and Lokitz B S 2018 *J. Polym. Sci.* **56** 1346
- [27] Blake D M, Moens L, Rudnicki D and Pilath H 2005 *J. Sol. Energy Eng.* **128** 54
- [28] Daschner R, Greppmaier U, Kokelmann M, Rudolf S, Rudolf R, Schleeauf S and Wrobel WG 2017 *Biomed. Microdevices* **19** 7
- [29] Hemmerich KJ 1998 *Med. Plast. Biomater.* **5** 16
- [30] *ASTM International* 2002 ASTM F1980-02
- [31] Uchida T, Nitta M and Kanashima S 2015 *J. Photopolym. Sci. Technol.* **28** 261
- [32] Matsuo T, Sakurai M, Terada K, Uchida T, Yamashita K, Tanaka T and Takarabe K 2019 *Adv. Biomed. Eng.* **8** 137
- [33] Baikie I D, Smith P J S, Porterfield D M and Estrup P J 1999 *Rev. Sci. Instrum.* **70** 1842
- [34] Sarikaya Y, Önal M, Pekdemir AD 2020 *Clay Minerals* **55** 96
- [35] McNab J and Sandborg A *The EDAX EDITOR* **14** 37
- [36] Okawa H, Sampath A P, Laughlin S B and Fain G L 2008 *Current Biology.* **18** 1917